

Plugging by hydrodynamic bridging during flow of stable colloidal particles within cylindrical pores

By VENKATACHALAM RAMACHANDRAN
AND H. SCOTT FOGLER†

Department of Chemical Engineering, University of Michigan, Ann Arbor, MI 48109, USA

(Received 4 November 1997 and in revised form 11 November 1998)

This paper describes the flow-induced retention of charge stabilized colloidal particles during flow through cylindrical pores. Current models describing the low-Reynolds-number flow behaviour of particulate suspensions through porous media do not predict retention of stable colloidal particles if the particles are smaller in size than the pores, and the particles and the pores have like surface charges. Retention is not expected under these conditions because the small particle size relative to the pore constriction size precludes straining (physical capture of particles larger than the pore constriction) while particle–pore surface electrostatic repulsion prevents deposition. However, the experiments show that substantial particle retention can occur under these conditions. The mechanism causing particle retention under these conditions, hydrodynamic bridging, is flow-induced. In this mechanism, hydrodynamic forces acting on particles arriving at a pore entrance do not allow their simultaneous passage through the pore, resulting in the formation of a particle bridge across the pore constriction. This paper reports experiments elucidating the effects of velocity, particle concentration, and the ratio of pore size to particle size on retention by hydrodynamic bridging. For flow through cylindrical pores, the effect of velocity on retention by bridging is opposite to that of retention by deposition. Furthermore, observations indicate the existence of a critical flow velocity necessary for particle bridging to occur. This critical velocity is a measure of the net colloidal interparticle and particle–porous medium repulsion that must be overcome by the hydrodynamic forces for bridging to occur. Approximate theoretical calculations of the trajectories of two particles approaching an isolated cylindrical pore are also presented. These calculations show that bridging is indeed possible in the Stokes flow regime for the experimental conditions considered.

1. Introduction

The retention of colloidal particles from a liquid suspension during flow through porous media is of fundamental importance to many engineering and natural systems. For example, flow behaviour of colloidal particles plays a significant role in transport and containment of contaminants in ground waters (McCarthy & Wobber 1993; Tadros & Gregory 1994), formation damage due to particulate plugging during enhanced oil recovery (Porter 1989), and filtration based solid–liquid separation techniques used in the biochemical and the chemical process industries (Scott 1990).

† Author to whom correspondence should be addressed.

A fundamental understanding of the different mechanisms by which flowing particles are retained within porous media is imperative for the efficient design and control of these processes.

A colloidal suspension consists of micron or submicron sized particles dispersed in a liquid. The term 'stable' refers to the ability of the particles in the suspension to remain dispersed and resist flocculation. During suspension flow through a porous medium, particles can interact with the medium either individually or collectively by different mechanisms that may lead to their retention. Up until now, straining and deposition are considered to be the primary mechanisms by which particles are retained. Straining or size exclusion refers to the capture of a particle at a pore constriction that is smaller in size than the particle. If the particles are smaller in size than the pores, they can penetrate the porous medium. While flowing within the individual pores, particles can be deposited on the pore surface by different mechanisms such as inertial impaction, interception, Brownian diffusion, and sedimentation (Tien 1989). In capture by inertial impaction, inertia causes particles to deviate from fluid streamlines and leads to deposition on the pore surface. When a particle travels along a streamline that is less than a particle radius away from the collector surface, it can be retained owing to interception. For submicron particles, Brownian diffusion can play a significant role in particle transport to the pore surface. Under conditions where gravity forces are significant (large and/or dense particles), particles can be also retained by sedimentation. The efficiency of particle deposition by these mechanisms is significantly affected by surface forces such as dispersion and electrostatic forces, and forces due to lyophobic/lyophilic interactions between the particles and the pore surface.

The list of classical capture mechanisms described above is incomplete in that it does not include the mechanism of hydrodynamic bridging in which particle retention is induced solely by hydrodynamic forces during the low-Reynolds-number flow of stable colloidal suspensions (fluid and particle inertia insignificant). The most widely recognized aspect of particle-pore wall hydrodynamic interaction during particle capture from low-speed flows is the resistance to capture under conditions of net attraction between the particle and the pore wall (Spielman 1977). This resistance to capture arises owing to the slow drainage of the liquid (suspending medium) from the gap between the particle and the collector at small distances of separation (Charles & Mason 1960). The fact that hydrodynamic forces acting on a particle can lead to capture under conditions of net repulsion has not been investigated.

Hydrodynamic bridging is the phenomenon of blocking of pores by simultaneous arrival of stable particles whose sizes are smaller than the pore size. At a sufficiently high flow velocity, hydrodynamic forces at the pore entrance can overcome interparticle and particle-pore surface electrostatic repulsion, resulting in the formation of a particle bridge across the pore entrance (in the absence of particle inertia). Under suitable conditions, hydrodynamic bridging can cause severe, unexpected plugging of porous media.

A particle suspended in a fluid undergoing low-Reynolds-number flow experiences two different forces owing to the fluid motion: one is the applied shear force which acts to move the particle in the direction of the pressure gradient, and the other is the drag force opposing relative motion between the particle and the fluid. In the absence of inertia, the sum of these two forces is zero and it is the balance between these forces that determines the particle velocity. However, if there are non-hydrodynamic (e.g. colloidal) interactions between the flowing particle and another particle or the porous medium, the net hydrodynamic force is non-zero. In this paper, the term

'hydrodynamic force' refers to the net hydrodynamic force acting on the particle while recognizing that the applied shear force is the component responsible for the phenomenon of bridging. Flow-induced particle retention is qualitatively similar to the phenomenon of shear-induced flocculation of stable particles. The stability of colloidal dispersions in different unbounded flow fields has been extensively studied (van de Ven & Mason 1976; Zeichner & Schowalter 1977; Melik & Fogler 1988).

This paper describes the retention of stable colloidal particles by the mechanism of hydrodynamic bridging during flow through cylindrical pores. The experiments are classified into two different regimes. Experiments in regime I demonstrate particle retention by hydrodynamic bridging. The effects of particle concentration and aspect ratio (ratio of pore size to particle size) on bridging are described. Experiments in regime II demonstrate the difference in the nature of retention by bridging and deposition by studying the effect of velocity on deposition. In all the experiments, the Reynolds number for suspension flow within pores based on the particle size or the pore size is very small ($Re < 0.01$). Approximate calculations of trajectories of two particles approaching an isolated cylindrical pore under the influence of hydrodynamic and colloidal forces support experimental observations.

The organization of the paper is as follows: after describing the experimental system, experimental observations for regimes I and II are presented and described. Finally, calculations describing the motion of two particles approaching a cylindrical pore are presented.

2. Experimental system

2.1. Porous medium

Nuclepore[®] track-etched polycarbonate membranes having straight cylindrical pores were obtained from Corning Costar Corporation (Acton, MA). Figure 1 shows a scanning electron micrograph of the membrane. The porous structure in track-etched materials is obtained by preferentially etching tracks created by the passage of heavily ionizing, nuclear particles (Fleischer, Price & Walker 1975). These tracks are characterized by intense damage on an atomic scale and can be etched by a properly chosen chemical reagent. Circular membranes of size 25 mm and pore sizes 1 μm , 2 μm , and 3 μm were used. The membrane thickness specified by the manufacturer is 10 μm . Examination of the membrane surface using the scanning electron microscope (SEM) revealed that the pore structure is not entirely regular. There is a distribution of pore sizes together with the presence of a significant number of overlapping pores ($\sim 14\%$). Table 1 lists the two nominal pore sizes used, and the measured average pore size and standard deviation determined from SEM micrographs. Similar observations for Nuclepore[®] membranes have been reported by Liabastre & Orr (1978) and Martínez-Villa, Arribas & Tejerina (1988). It was also evident from the micrographs that the pores are not perfectly straight. The maximum deviation of the pore axis from the normal to the membrane surface is reported by the manufacturer to be 35° . For a membrane thickness of 10 μm , this deviation implies that interconnection between pores will be present in the membrane. Martínez-Villa *et al.* (1988) have reported that the pore number densities determined for the two sides of a membrane are not significantly different. This observation indicates that the number of pores that do not penetrate the entire thickness of the membrane is very small.

Keesom, Zelenka & Radke (1988) have measured the pore surface zeta potential using the streaming potential technique. They report that the pore surface is negatively

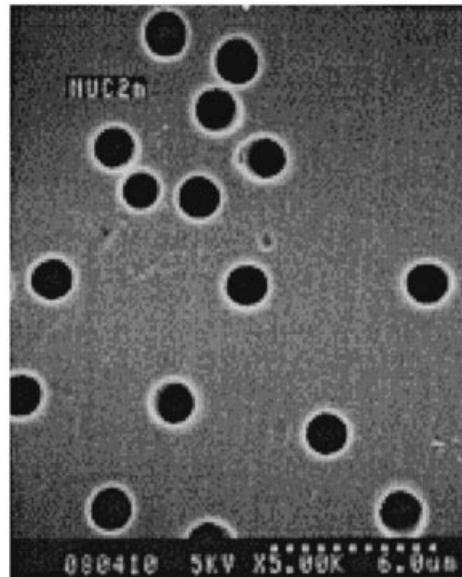


FIGURE 1. SEM picture of 2 μm pores in a Nuclepore[®] track-etched membrane (entrance face of the membrane shown at $\times 5\text{K}$).

Nominal pore size (μm)	Measured pore size (μm)	% Standard deviation
1	0.82	20.3
2	1.65	13.7
3	2.76	15.5

TABLE 1. Pore sizes in Nuclepore[®] membranes used.

charged owing to the dissociation of carboxyl groups on the surface. The maximum value of the pore zeta potential is about -27mV for pH values above 6 and an ionic strength of 10^{-3}M KCl. The pore surface is hydrophobic in nature owing to the polycarbonate material of the membrane (Bisio *et al.* 1980).

2.2. Particles

Charged polystyrene microspheres dispersed in water were used in the experiments. Strong interparticle electrostatic repulsion arising from the interaction of charged groups present on the surface of particles imparts stability to the suspension. Figure 2 shows a micrograph of particles used. Table 2 lists the latex particles used and their properties. Concentrated particle suspensions were purchased from Interfacial Dynamics Corporation (Portland, OR) and diluted as necessary for use in the experiments. According to the manufacturer, the particles are prepared without the use of surfactants and are rigid because polystyrene is an amorphous polymer with a high glass transition temperature. Transmission electron microscopy (TEM) was used to determine the size distribution of the particles. TEM micrographs show that the particle cross-section is perfectly circular and that the particle surface is smooth at the magnification used ($\times 40\,000 - \times 80\,000$). The particle zeta potentials were measured

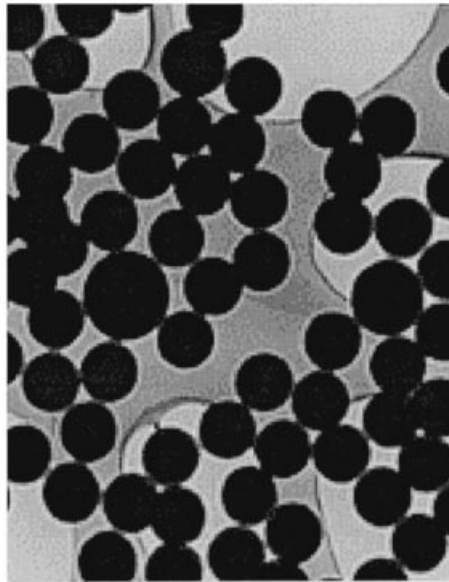


FIGURE 2. TEM picture showing 0.25 μm latex particles ($\times 50\text{K}$).

Particle type	Surface properties	Nominal diameter (nm)	Surface charge density ($\mu\text{C cm}^{-2}$)
Polystyrene sulfate (PSS)	Negatively charged, hydrophobic	241, 249	-1.7, -2.0
Polystyrene carboxylate (PSC)	Negatively charged, hydrophilic	220	-141
Polystyrene amidine (PSA)	Positively charged, hydrophobic	188	+8.3

TABLE 2. Properties of latex particles in experiments.

with a Pen Kem 501 Laser Zee Meter which operates based on the technique of microelectrophoresis.

2.3. Experimental set-up and procedure

Particle retention within the membrane pores was monitored by measuring the pressure drop across the membrane housed in a filter holder (figure 3). A sensitive differential transducer capable of measuring a pressure drop as small as 10 Pa was used. The suspensions were injected through the membrane at constant volumetric flow rates using an ISCO-500D syringe pump. The pump is capable of pulse-free injection over a wide range of flow rates.

To reduce the polydispersity in particle size, the suspensions were prefiltered prior to use in experiments. The extent of prefiltration depended on the pore size in the membrane to be used in the experiment. For example, for flow through a 1 μm pore membrane, particles were prefiltered four times using 1 μm filters and four times using 0.8 μm filters. The prefiltration was performed at very low flow rates and using large filters (90 mm size) to maximize the filtration area. To prevent bacterial growth, 50 p.p.m. of the biocide sodium azide was added to the suspensions. Dissociation of

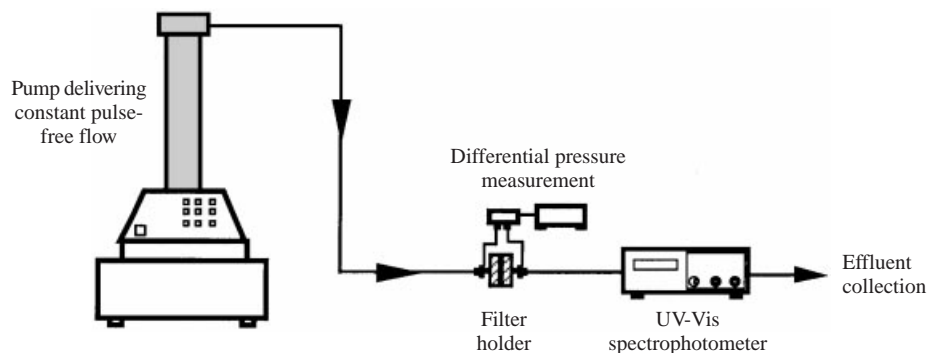


FIGURE 3. Apparatus set-up for flow experiments.

sodium azide (NaN_3) results in a background ionic strength of $8 \times 10^{-4} \text{ M Na}^+$ and N_3^- ions, respectively.

The filter holder with the membrane was vacuum saturated with deionized water to remove air. Prior to suspension injection, the pressure drop across the membrane was determined for three different flow rates of deionized water having the same ionic strength and pH as the suspension. The choice of flow rates depended on the flow rate at which the suspension was to be injected. This step is essential since the measured pressure drop during suspension flow is normalized with the pressure drop during the flow of water for meaningful representation of the experimental data. At the end of each experiment, the membranes were examined using the SEM to observe the nature of particle retention within pores. Membrane preparation for SEM observation involved cleaning by immersing the membrane in the particle-free dispersion medium (deionized water having the same ionic strength and pH as the suspension in the experiment). This procedure removed the thin film of suspension present on the membrane surface while preserving the particles retained during flow. The gentle cleaning procedure does not disturb the retained particles because they are usually in primary minimum contact with the membrane surface. Visual examination aided in correctly interpreting the particle flow behaviour from the pressure drop data.

3. Experimental results and discussion

The experiments have been classified into two distinct regimes depending on the nature of the interparticle and particle-pore surface colloidal interactions. It is important to note that in all experiments, (i) particle retention by straining is insignificant because the particles are smaller in size than the pores, (ii) the particle suspension is stable to flocculation by Brownian collisions, and (iii) particle inertia does not play a role in retention owing to the very small Reynolds numbers (Re range: 0.0001–0.01).

3.1. Regime I

Experiments in regime I are characterized by the following conditions: a strong interparticle colloidal repulsion, a strong particle-pore surface colloidal repulsion, and an aspect ratio of 3–4.

The aspect ratio is defined as the ratio of the nominal pore size to the nominal particle size. Under these conditions, particle straining will be insignificant as the small particle size ensures passage of particles through the pores without capture.

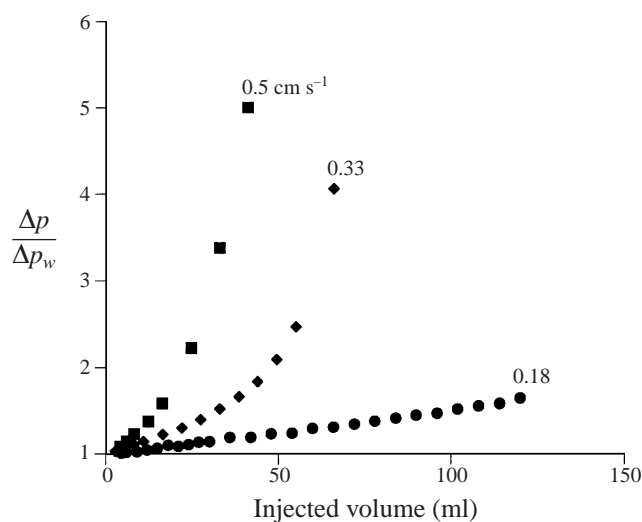


FIGURE 4. Effect of velocity on particle retention in regime I ($0.25 \mu\text{m}$ PSS latex spheres). Aspect ratio 3.3; 1235 p.p.m.

Further, particles will not deposit within pores because of the strong particle–pore surface repulsion and the absence of particle inertia. Negatively charged particles were used at a suspension pH of 6 which ensured fully charged particle and pore surfaces. The low electrolyte concentration ($< 0.001 \text{ M Na}^+$ owing to addition of NaN_3) in the suspension ensured strong interparticle and particle–pore surface electrostatic repulsion.

3.1.1. Effect of velocity

Figure 4 shows the effect of velocity on particle retention at a fixed particle concentration during the flow of $0.249 \mu\text{m}$ diameter PSS particles through $1 \mu\text{m}$ pores (aspect ratio of 3.3). In this figure, the normalized pressure drop across the membrane during suspension flow is shown as a function of the total volume of suspension injected. The normalized pressure drop is the ratio of pressure drop across the membrane during suspension flow to that during the flow of deionized water ($\Delta p/\Delta p_w$). Because the particle concentration is fixed in these experiments, the numerical values on the X-axis are proportional to the total number of particles injected. The velocities specified are the initial interstitial velocities.

In figure 4, the increase in the normalized pressure drop during suspension flow indicates that particles are being retained in spite of the fact that straining and deposition are insignificant. The mechanism of particle retention under these conditions is hydrodynamic bridging. During bridging, particles plug pores by forming a bridge across the pore entrance (figure 5). The bridge formation is due to hydrodynamic forces in the vicinity of the pore overcoming interparticle and particle–pore surface colloidal repulsion and preventing the particles from simultaneously flowing into the pore. Though the possibility of particle retention by this mechanism has been recognized in earlier studies (Muecke 1979; Khilar & Fogler 1984; Vitthal & Sharma 1992), the phenomenon has not been clearly understood.

The effect of velocity on retention by bridging is unique to this mechanism. One observes from figure 4 that, as the velocity is increased, the rate, as well as the extent of plugging of the membrane, increases for the same number of particles injected. In

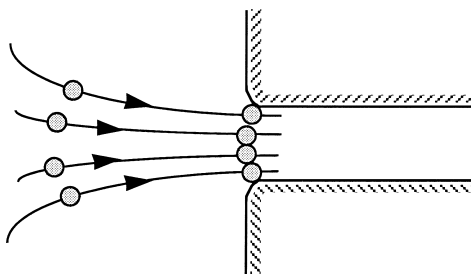


FIGURE 5. Particle capture by hydrodynamic bridging.

other words, the efficiency of particle retention by hydrodynamic bridging increases with increasing flow velocity. Note that the curves for the different velocities would coincide for a fixed particle concentration if particles were retained by straining. On the other hand, it will be shown from experiments in regime II that the effect of velocity on deposition is opposite to that observed for retention by bridging.

Bridging requires the simultaneous arrival of particles at the pore entrance at the correct spatial locations with sufficient velocities. For dilute suspensions and low Reynolds numbers, particles far away from the pore will follow fluid streamlines. In the vicinity of the pore, however, the particle starts to deviate from the fluid streamline owing to interactions with other particles and the pore wall. The tendency of the particle to move away from neighbouring particles and the pore wall owing to net colloidal repulsion is resisted by the hydrodynamic force acting on it. If the magnitude of the hydrodynamic force is sufficient to overcome the repulsion, bridging will occur.

Figure 6 shows SEM pictures of typical membrane pores for the case of a high flow velocity. The micrographs show particle bridges across pore entrances. Bridges were not observed in all the pores. In a few of the pores, particles were present in the vicinity of the pore entrance both inside and outside the pores. It is possible that while drying the membrane, strong capillary forces acting on particles dislodged bridges which were not mechanically strong. (In a strong bridge, particles are expected to be lodged such that the rolling of particles in contact with the pore edge is not possible. If the particles contacting the pore edges can move by rolling during drying, break-up of the bridge will occur.) It is evident from the micrographs that particle deposition is absent as particles have been retained only at the pore entrance. If deposition had occurred, particles adhering to the membrane surface would have been present both within pores and on membrane faces (compare with figure 15). It can be seen from figure 7 that pore bridging is not occurring at very low velocities in regime I.

Critical velocity. The explanation of the phenomenon of bridging implies the existence of a critical velocity below which bridging will not occur since hydrodynamic forces at the pore entrance have to overcome a certain magnitude of the net colloidal repulsion between particles for particle bridging. The magnitude of this critical velocity will depend on the aspect ratio, flow geometry, surface properties of pore and particle, ionic strength, and pH. (The ionic strength and pH affect the magnitude of the electrostatic repulsion.) The trend of increasing extent of plugging with increasing velocity observed in figure 4 supports the notion of a critical velocity for bridging to occur. The absence of retention by bridging at a low velocity can be seen more clearly in figure 8 where an experiment was performed at a velocity of 0.024 cm s^{-1} . In the experiments in figure 8, PSC latex particles with a size of $0.22 \mu\text{m}$ and membranes

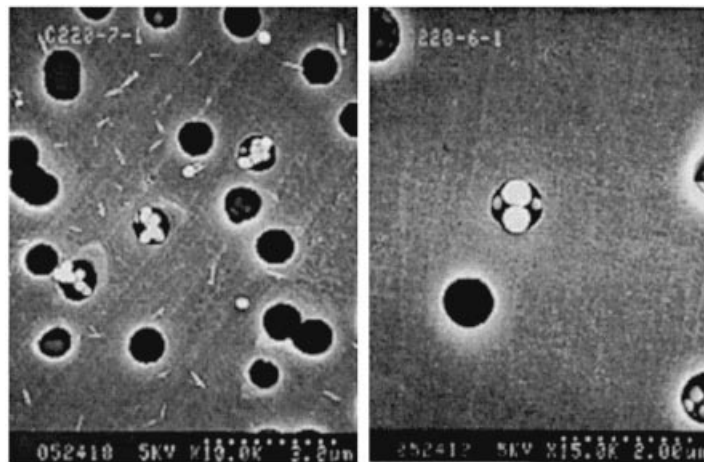


FIGURE 6. Particle bridging at a high velocity regime I.

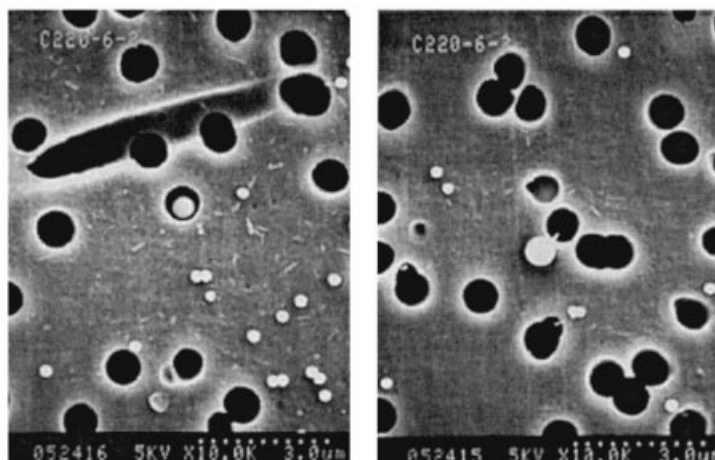


FIGURE 7. Absence of particle retention at very low velocities in regime I.

with $1\ \mu\text{m}$ pores were used (aspect ratio of 3.7). For the run at $0.024\ \text{cm s}^{-1}$, the normalized pressure drop initially increases and then remains constant as suspension is injected indicating the absence of particle retention. The normalized pressure drop initially increases to 1.04 because of particle straining due to a small overlap in the particle and pore size distributions. Straining is, however, insignificant since the pores capable of straining particles are relatively few in number. The degree of plugging in experiments in figure 8 is less than that in experiments using PSS latex shown in figure 4 because of the lower particle concentration and the higher charge of PSC latex (the electrostatic repulsion is stronger).

Further evidence for the existence of a critical velocity for bridging is shown in figure 9. In this experiment, the suspension initially flowed through the membrane at a very low rate during which the normalized pressure drop remained constant, indicating the absence of particle retention by bridging. After the flow of about 125 ml of suspension through the membrane, the flow rate was increased significantly and a continuous increase in the pressure drop across the membrane occurred owing to

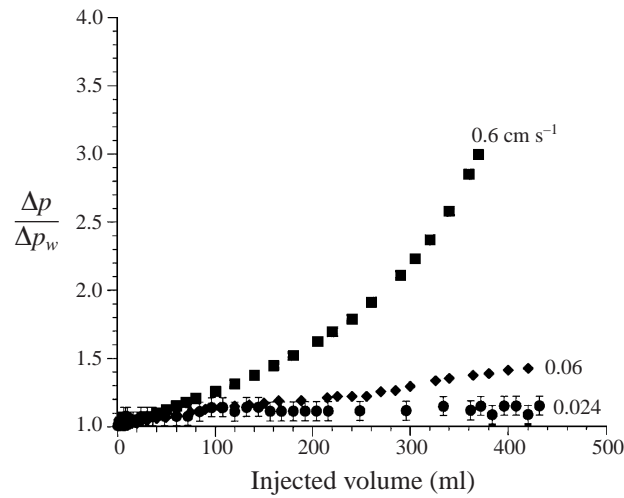


FIGURE 8. Effect of velocity on hydrodynamic bridging ($0.22 \mu\text{m}$ PSC latex spheres). Aspect ratio 3.7; 415 p.p.m.

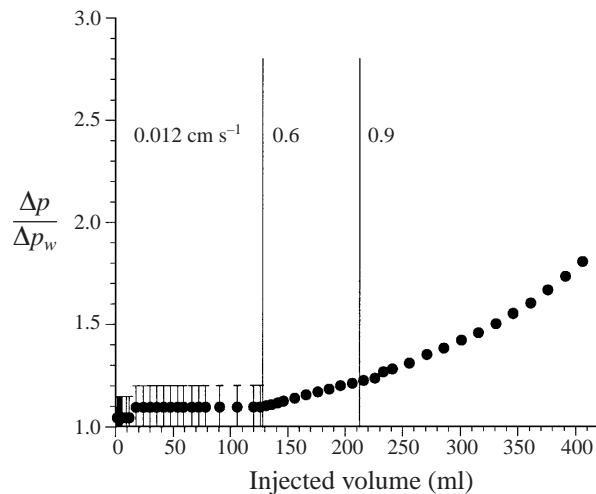


FIGURE 9. Existence of a critical velocity for hydrodynamic bridging ($0.241 \mu\text{m}$ PSS latex spheres). At the low flow rate, uncertainty in the magnitude of the pressure drop is large owing to the small pressure drop. Aspect ratio 3.4; 525 p.p.m.

particle bridging. Increasing the flow rate further resulted in a greater rate of plugging of the membrane pores.

Other relevant phenomena involving colloidal and hydrodynamic forces that exhibit a critical velocity are the detachment of deposited colloidal particles (Gruesbeck & Collins 1982; Das, Schechter & Sharma 1994) and the entrance of a charged particle into a charged pore during ultrafiltration (Bowen & Sharif 1996).

Particle inertia. The Stokes number (St) characterizing particle motion which is the ratio of viscous to inertial forces is a measure of the importance of particle inertia. It is defined as the ratio of the characteristic time spent by the particle in the vicinity of the collector to the characteristic time required for the particle to be transferred to the collector surface owing to inertia and is given by (Russel, Saville & Schowalter

1989):

$$St = \frac{2}{9} \left(\frac{d_p}{a} \right)^2 \frac{\rho_p}{\rho} Re.$$

Here d_p is the pore diameter, a is the particle diameter, ρ_p and ρ are the particle and fluid densities respectively, and Re is the Reynolds number ($Re = \rho \bar{v} d_p / \mu$ where \bar{v} is the average interstitial velocity within the pore and μ is the fluid viscosity). Kao *et al.* (1988) studied the capture of particles by inertial impaction during flow through Nuclepore[®] type filters, taking into account the hydrodynamic interaction of the particle with the entrance geometry of the pores. They have shown that for very low values of the Stokes number, which is the case when particle inertia is insignificant, inertial impaction of particles onto the pore edges is not possible, even in the absence of electrostatic repulsion. The maximum value of the Stokes number in the experiments is about 10^{-4} . Consequently, particle retention in the experiments is not occurring by inertial impaction of particles onto the pore surface.

Internal plugging. The only mechanism by which discrete (non-aggregated) flowing particles can internally plug a pore is dendrite formation (Davis 1973; Payatakes & Gradon 1980). Dendrite formation is initiated when flowing particles deposit on the pore wall by interception or inertial impaction. Dendrite growth takes place by the retention or capture of flowing particles on previously retained particles, by the mechanisms of inertial impaction and/or interception. However, neither interception nor inertial impaction can occur in experiments in regime I, because the strong interparticle and particle–pore repulsion prevents interception while the domination of viscous forces over inertial forces prevents inertial impaction. In fact, dendrite formation has only been observed during aerosol flow where inertia dominates and electrostatic repulsion is insignificant. Therefore, internal plugging by dendrite formation is absent in the system.

Internal plugging is also possible if particles can flocculate within the pores (shear-induced flocculation) and subsequently block them. As a consequence of the converging nature of the flow into the pore, the magnitude of the hydrodynamic forces acting to push two particles together is greatest at the pore entrance. Because the pores in the membrane have a uniform cross-section throughout their length (for the pore sizes used in the experiments, comparison of the pores size distribution determined at both faces of the membrane did not show any difference), aggregation of the particles within the pore is not expected for conditions when the hydrodynamic forces at the pore entrance are insufficient to cause bridging. This has been verified by estimating the extent of flocculation possible for the experimental conditions using theoretical results available for shear-induced flocculation during suspension flow within capillary tubes (Gregory 1981a, 1982). The calculations show that under the conditions of the experiment virtually no flocculation will occur within pores in the system (see Appendix A). Particle bridging at the intersection of two pores within the membrane is unlikely because a change in direction of flow occurs only at such a junction.

3.1.2. Effect of particle concentration

The effect of particle concentration on particle retention for an aspect ratio of 3.3 is shown in figure 10. In these experiments, 0.249 μm PSS particles and membranes with 1 μm pores were used. The effect of increasing the particle concentration on any capture mechanism is to increase the rate of retention. For straining and particle deposition at low surface coverage, the rate of retention is proportional to the particle concentration for dilute suspensions. However, both straining and particle

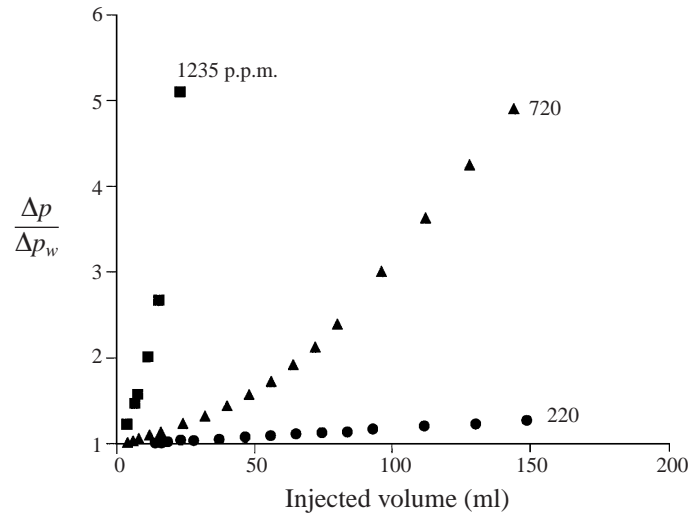


FIGURE 10. Effect of concentration on hydrodynamic bridging ($0.25 \mu\text{m}$ PSS latex spheres). Aspect ratio 3.3; 0.48 cm s^{-1} .

deposition are insignificant in experiments in regime I. It can be seen from figure 10 that the rate of plugging of the membrane increases with increasing particle concentration for a given suspension flow rate. This trend is due to the fact that at the higher concentrations, a greater number of particles arrive at the pore entrance, which increases the probability of particles being at the correct spatial locations for bridge formation. Note that in the results shown in figure 10, the total number of particles that have passed through the pores is different for each run since the particle concentrations are different. A better representation of the data is shown in figure 11 where the results in figure 10 have been replotted in terms of total number of particles injected. Figure 11 clearly shows that the rate of plugging by bridging has a nonlinear dependence on particle concentration. For a mechanism that depends linearly on concentration, such as straining, the curves in figure 11 would coincide.

Although the rate of retention by bridging decreases with decreasing particle concentration (as seen in figure 10), for velocities greater than or equal to the critical velocity, a non-zero probability for bridge formation exists even for low concentrations. In that sense, bridging does not have a critical dependence on particle concentration.

3.1.3. Effect of aspect ratio

Figure 12 shows the dependence of hydrodynamic bridging on the aspect ratio at low and high velocities for $0.241 \mu\text{m}$ sulfate latex suspension through $1 \mu\text{m}$, $2 \mu\text{m}$ and $3 \mu\text{m}$ pore membranes. During bridging, the number of particles of average size required to bridge pores of average size is equal to the aspect ratio. Because the probability of the required number of particles arriving simultaneously at the pore entrance at the correct spatial locations decreases with increasing aspect ratio, retention by bridging becomes insignificant at a sufficiently high aspect ratio. The extent of plugging by bridging will therefore decrease as the aspect ratio increases, as seen in figure 12. Apart from the geometrical considerations described above, the aspect ratio also affects bridging by being one of the main parameters that determines the magnitude of the critical velocity for bridging.

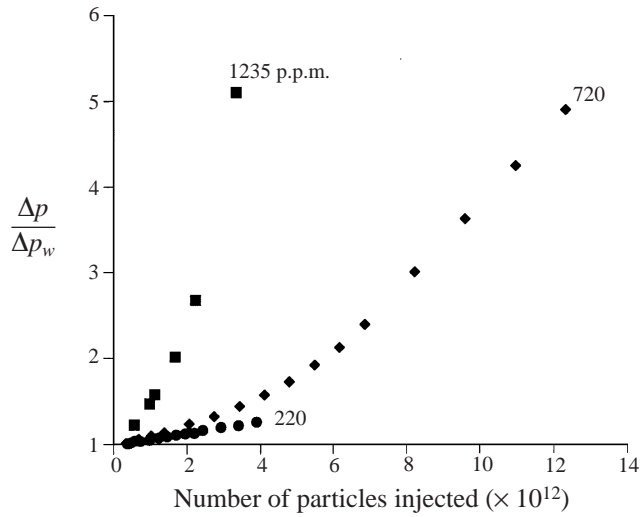


FIGURE 11. Nonlinear dependence of rate of retention by bridging on concentration (same data as in figure 4).

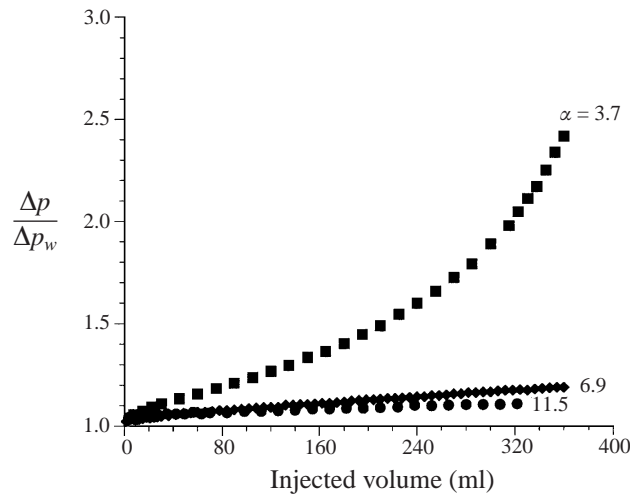


FIGURE 12. Effect of aspect ratio (α) on particle retention by bridging. 0.241 μm PSS; 650 p.p.m.; 0.9 cm s^{-1} .

3.2. Regime II

The focus of experiments in this regime is to study the effect of velocity on particle deposition. By comparing these experimental observations with those in regime I, the difference between the effect of velocity on hydrodynamic bridging and the effect of velocity on deposition will be demonstrated. Experiments in this regime are characterized by the following conditions: strong particle-pore surface attraction, strong interparticle repulsion, large aspect ratio, and low particle concentration.

Experiments were performed with positively charged 0.188 μm polystyrene amidine latex particles and 2 μm pore membranes (aspect ratio = 8.7). The solution pH was adjusted to 4 to ensure suspension stability. The conditions chosen are conducive for particle deposition owing to the strong attraction between particles and the pore

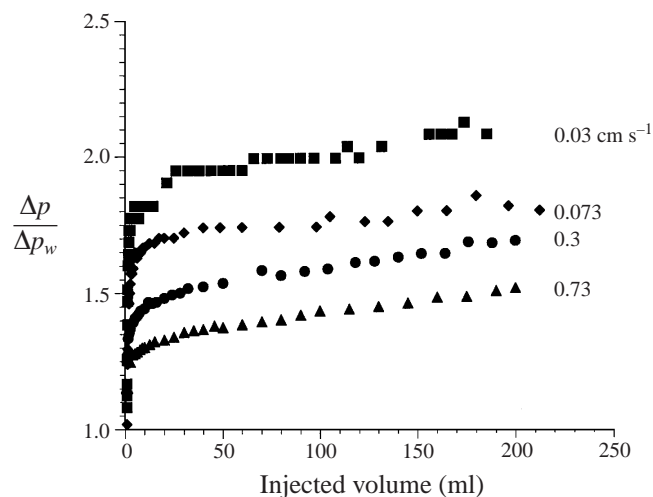


FIGURE 13. Effect of velocity on deposition ($0.188\ \mu\text{m}$ positively charged amidine latex spheres). Aspect ratio 8.7; 120 p.p.m.

surface. A large aspect ratio and low particle concentration were intentionally chosen to ensure that hydrodynamic bridging was insignificant in these experiments.

The effect of velocity on deposition is shown in figure 13. In each experiment in figure 13, the rate of increase in the normalized pressure drop is initially rapid but quickly decreases to virtually zero, leading to a final, steady pressure drop across the membrane. It can also be seen from figure 13 that the final normalized pressure drop reached in the experiments decreases as the flow velocity is increased. This implies that the extent of particle retention decreases with increasing velocity in regime II, which is opposite to that observed for retention by hydrodynamic bridging in regime I. This behaviour is consistent with deposition being the mechanism of particle retention in experiments in regime II.

The initial rapid increase in the normalized pressure drop is due to rapid deposition of particles within pores resulting from the strong particle-pore surface attraction. Particles deposited within a pore decrease the effective pore size and therefore increase the pressure drop across the pore. The decrease in the rate of particle deposition with time is due to depletion of the pore surface area available for deposition. Because of the presence of strong interparticle repulsion, only a single layer of particles is expected within the pores (see figure 14*a*). In these experiments, the normalized pressure drop attained a final steady value indicating that multilayer particle deposition is not occurring. The fact that only a single layer of particles is present within the pore can be verified by comparing the observed maximum increase in pressure drop with that expected, assuming that the pore radius is reduced by one particle diameter after particle deposition. Based on Poiseuille flow through a cylindrical channel, the normalized pressure drop across the membrane is expected to increase by a factor $(1 - 2/\alpha)^{-4}$ owing to particle deposition, which for an aspect ratio of 8.7 is 2.84. This expected value is, however, an over-estimate because the deposited particles are spherical in shape and the pore radius is not reduced by one particle diameter uniformly along the length of the pore. The actual increase in pressure drop will therefore be less than 2.84, which is indeed the case in the experiments where the maximum observed value is about 2.2.

The trend of decreasing deposition with increasing velocity can be explained based

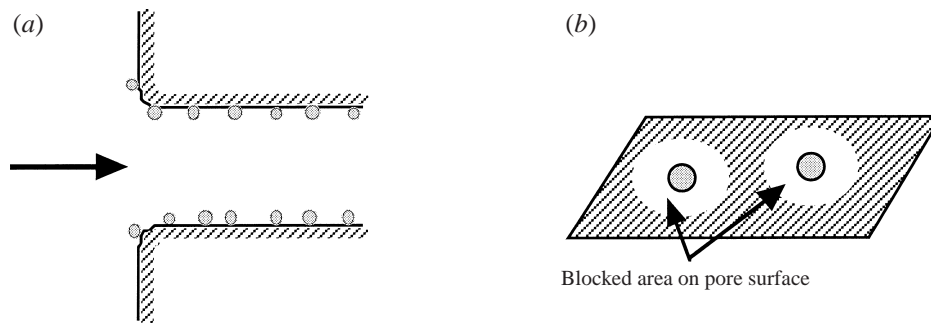


FIGURE 14. (a) Deposition of particles as a single layer within pores (regime II); (b) blocking by deposited particles.

on the effect of velocity on blocking by deposited particles. The term blocking, in the context of particle deposition, refers to the loss of pore surface area surrounding a deposited particle that is available for further deposition and not the plugging of pores by particles (see figure 14*b*). Blocking occurs owing to two independent interactions between a flowing particle and a deposited particle: strong interparticle colloidal repulsion, and interparticle hydrodynamic interaction. For sufficiently high flow intensities, direct experimental observations of particle deposition (Meinders, Noordmans & Busscher 1992; Adamczyk *et al.* 1994) as well as theoretical calculations (Dabros 1989; Adamczyk, Siwek & Szyk 1995) show that the area blocked by a deposited particle is asymmetric with respect to the direction of flow. Therefore, the blocked area downstream of the particle is larger than that on the upstream side. As a result of asymmetric blocking by deposited particles, the total pore surface area available for deposition – and therefore the total number of particles – decreases as velocity increases.

Figure 15 compares SEM photographs of typical pores in the membranes used in the 0.03 cm s^{-1} and 0.73 cm s^{-1} runs in figure 13. These photographs confirm that the particles are retained in a single layer within the pores. It can also be seen that fewer particles have been deposited within pores at the higher velocity. This observation is consistent with the decrease in the final pressure drop upon increasing the velocity in the experiments.

4. Particle trajectories near a pore entrance

The purpose of the calculations in this section is to determine whether hydrodynamic bridging can occur for the experimental conditions in regime I. For retention by bridging, it is necessary for the hydrodynamic forces acting on the particles at the pore entrance to overcome net interparticle colloidal repulsion. The hydrodynamic and colloidal forces acting on the particles as they approach a pore will be compared to ascertain whether bridging is possible. For dilute suspensions and low Reynolds numbers, the hydrodynamic force acting on a particle far away from a pore is zero because both interparticle interactions and particle inertia are negligible. In the vicinity of the pore, however, the hydrodynamic force acting on the particle is non-zero because of the interparticle and particle–pore colloidal interactions. For neutrally buoyant particles, the total force acting on the particle is zero which implies that the hydrodynamic force acting on a particle is equal in magnitude to the colloidal force acting on it. An order of magnitude comparison of the forces is therefore not

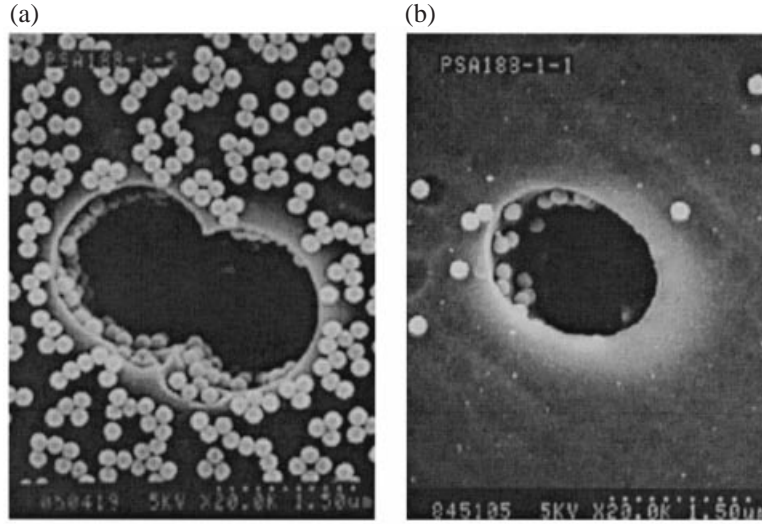


FIGURE 15. SEM micrographs comparing particle deposition within pores at (a) 0.03 cm s^{-1} and (b) 0.73 cm s^{-1} for an aspect ratio of 8.7. The membranes are from experiments shown in figure 13.

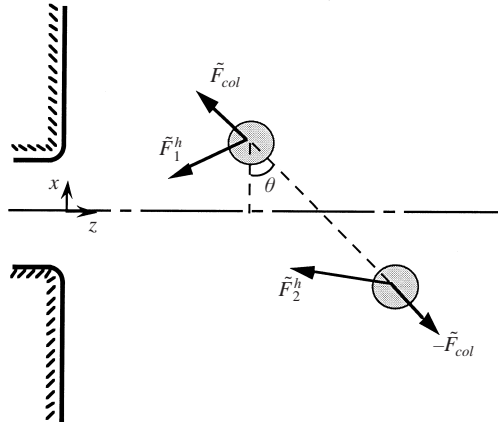


FIGURE 16. Particles-pore system for trajectory calculations.

possible because the magnitude of the hydrodynamic force acting on a particle near the pore entrance depends on the net colloidal force acting on it.

The procedure adopted for determining the possibility of bridging therefore involves first calculating the particle velocities near the pore entrance based on a force balance and then calculating the particle trajectories. From a knowledge of the trajectories, the interparticle separation as the particles approach the pore can be determined. When the interparticle separation approaches zero near the pore entrance, bridging is possible.

The system chosen in the calculations is shown in figure 16. The trajectories of two spherical colloidal particles approaching a cylindrical pore will be calculated. The trajectory equation governing the motion of a particle in any flow field in the symmetry plane (x, z) is given by

$$\frac{dx_i}{dz_i} = \frac{U_x^i}{U_z^i}, \quad (1)$$

where (x, y, z) are the Cartesian coordinates with the origin at the centre of the pore entrance, and \mathbf{U}^i is the velocity of the i th particle ($i = 1, 2$ here). The velocities of the particles can be obtained from the assumption that the net force acting on the particles at any instant is zero. (Under Stokes flow conditions, this pseudosteady state approximation is usually valid for submicron colloidal particles dispersed in water because the viscous relaxation time is very small (Russel *et al.* 1989).) A force and torque balance for the particle located above the pore axis ($x > 0$) in figure 16 is shown below:

$$F_x^h(U_x, U_z, \Omega) + F_{col} \cos(\theta) = 0, \quad (2)$$

$$F_z^h(U_x, U_z, \Omega) - F_{col} \sin(\theta) = 0, \quad (3)$$

$$T_y(U_x, U_z, \Omega) = 0. \quad (4)$$

The superscript ‘ h ’ and subscript ‘ col ’ denote that the force is of hydrodynamic and colloidal origin, respectively, θ is the angle between the line joining the centres of the particles and the vertical in the (x, z) -plane, and Ω is the angular velocity of the particle. For the particle located below the pore axis ($x < 0$), the signs of the colloidal force components in equations (2) and (3) will be reversed. This assignment is necessary because, by definition, the colloidal force is positive if the net interparticle interaction is repulsive, and negative if the interaction is attractive. Note that the pseudosteady state approximation also requires that the torque acting on each of the particles is zero (equation (4)). Simultaneous solutions of equations (2)–(4) will give the particle velocities required for calculating the trajectories.

4.1. Colloidal forces

For the particle–pore configuration being studied, the total colloidal force acting on a particle derives from both the interparticle and the particle–membrane colloidal interactions. The colloidal interaction energy between two charged particles dispersed in a polar liquid is a combination of three independent interactions: van der Waals attraction (for particles of the same material), electrostatic repulsion, and a short-range repulsion. The short-range repulsion is attributed to solvation or structural forces (Israelachvili 1985). These interactions can be quantified using a combination of the DLVO theory (Derjaguin & Landau 1941; Verwey & Overbeek 1948) and a mean potential formulation for the short-range repulsion (Feke *et al.* 1984).

The expression for the retarded London–van der Waals attraction between two spheres of equal size given by Schenkel & Kitchener (1960) has been used here:

$$V_A(h) = -\frac{Aa}{12h \left(1 + \frac{11.12h}{\lambda}\right)}, \quad (5)$$

where V_A is the attractive interaction energy, A is the Hamaker’s constant, h is the surface separation between the particles, λ is the characteristic wavelength of interaction (retardation length) often assumed to be about 100 nm, and a is the particle radius. The range of validity of this expression and its accuracy have been discussed by Gregory (1981*b*). The expression for the electrostatic repulsion between two identical colloidal particles used here is based on the linearized Poisson–Boltzmann equation and the Derjaguin approximation for constant potential interaction (Russel *et al.* 1988):

$$V_R(h) = 2\pi\epsilon a\psi_0^2 \ln(1 + e^{-\kappa h}), \quad (6)$$

where V_R is the electrostatic interaction energy, ϵ is the permittivity of water, ψ_0 is the

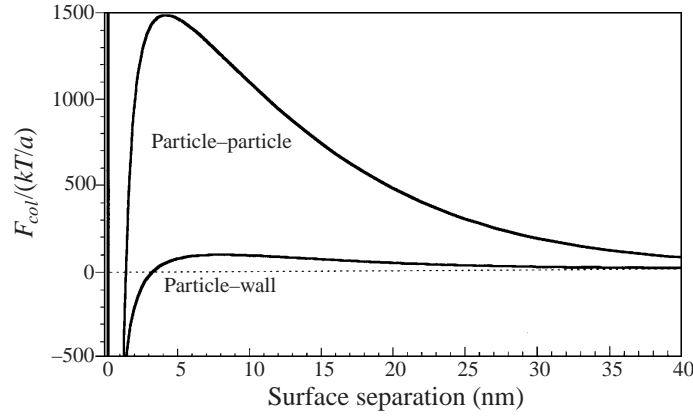


FIGURE 17. Comparison of the magnitudes of interparticle and particle–plane wall colloidal forces. In the vicinity of a pore, the particle–pore colloidal force will be less than that calculated based on the interaction between a particle and a solid plane wall. $\psi_{particle} = -50$ mV; $\psi_{wall} = -25$ mV; 0.001 M 1:1 electrolyte; pH = 6.

surface potential of the particles, and κ is the Debye–Huckel parameter (κ^{-1} is the screening length). For $\kappa a \approx 10$, which is the case in the experiments, the interparticle repulsive force calculated using equation (6) is within 10% of the exact force for $h \leq 3\kappa$ when the potential is small (Glendinning & Russel 1983). Feke *et al.* (1984) have derived an expression for the short-ranged Born repulsion between two identical spherical particles:

$$V_B(h) = \frac{A}{37800} \left(\frac{\sigma}{a}\right)^6 \frac{1}{R} \left\{ \frac{R^2 - 14R + 54}{(R-2)^7} + \frac{60 - 2R^2}{R^7} + \frac{R^2 + 14R + 54}{(R-2)^7} \right\}, \quad (7)$$

where V_B is the Born interaction energy, σ is the collision diameter (4 Å), and R is the centre to centre particle separation scaled using the particle diameter ($R = h/2a + 1$).

The total interparticle colloidal interaction potential, V_T , is the sum of the above three interaction potentials. The magnitude of the interparticle colloidal force, F_{col}^{p-p} , is related to V_T by the following equation:

$$|F_{col}^{p-p}(h)| = -\frac{d}{dh} V_T(h) = -\frac{d}{dh} [V_A(h) + V_R(h) + V_B(h)], \quad (8)$$

where the superscript $p-p$ denotes interparticle interaction. Figure 17 shows a plot of the interparticle colloidal force as a function of the separation distance. The parameters specified in figure 17 are the same as those used in the trajectory calculations. It can be seen that the interparticle interaction is strongly repulsive up to very small separations, where the dispersion attraction starts to dominate. For particles to associate near the pore entrance and bridge the pore, the repulsive force barrier seen in figure 17 has to be overcome. It should be noted that the interparticle potential energy for the specified conditions only exhibits a primary minimum because of the strong electrostatic repulsion. Systems where the interparticle potential is characterized by a primary minimum as well as a secondary minimum have not been considered.

For the case of a particle approaching a pore, as shown in figure 16, exact calculation of the colloidal interaction between the particle and the pore is not straightforward because of the geometry of the system (for example, see Bhattacharjee & Sharma (1995) for the van der Waals interaction and Bowen & Sharif (1997) for the electrostatic interaction between a particle and a charged pore in a charged

planar surface). In regime I, the magnitude of the particle pore–wall colloidal force is small compared to the interparticle colloidal force because the pore surface charge is smaller than that of the particles. In figure 17, the magnitude of the particle pore–wall colloidal force is compared with the interparticle colloidal force. The particle–pore wall colloidal force was calculated approximately based on the interaction between a spherical particle and a charged, solid plane wall (the charged, solid plane wall can be thought of as a sheet of the membrane material without pores). It can be seen that the maximum interparticle net repulsion is about 16 times greater than that between a particle and a solid plane wall. As mentioned previously, the hydrodynamic force acting on a particle is equal in magnitude and opposite in direction to the total colloidal force acting on it:

$$\mathbf{F}^h = -\mathbf{F}_{col} = -(\mathbf{F}_{col}^{p-p} + \mathbf{F}_{col}^{p-w})$$

where the superscript $p-w$ denotes particle–pore wall colloidal interaction. If the magnitude of the particle–pore wall colloidal force is small compared to the interparticle colloidal force, then the particle velocity as it approaches a pore will be determined primarily by the interparticle colloidal force, i.e. for $|\mathbf{F}_{col}^{p-p}| \gg |\mathbf{F}_{col}^{p-w}|$,

$$\mathbf{F}^h \approx -\mathbf{F}_{col}^{p-p}.$$

Therefore, the particle–pore wall colloidal interactions have been omitted in the calculations. The reader should note that the particle–membrane electrostatic repulsion is, however, sufficiently strong to prevent deposition in regime I.

4.2. Hydrodynamic force

Exact determination of the hydrodynamic forces acting on the particles requires solving the three-dimensional Stokes equations for fluid flow through the pore in the presence of the particles near the pore. The complex pore entrance geometry in the system, together with the presence of more than one particle near the pore during bridging, renders the solution to the equations very difficult and has not been attempted until now. In the last two decades, several workers have studied the hydrodynamic interaction between a finite sphere and a circular orifice for both flow through the orifice and past the orifice (for example, see Yan *et al.* 1987; Yan, Acrivos & Weinbaum 1991; Wu, Weinbaum & Acrivos 1992). The combined colloidal and hydrodynamic interaction between a sphere and a pore for axisymmetric motion of the sphere has also been studied (Hoffman & Stein 1992; Bowen & Sharif 1997). However, the case of simultaneously arriving particles at the entrance to a cylindrical pore has not been studied until now. While the Stokesian dynamics method has been successfully used to study the behaviour of a system of spherical particles in both unbounded (Brady & Bossis 1988) and bounded (Durlinsky & Brady 1989) flows, the presence of a discontinuous boundary (the pore entrance geometry) makes it difficult to use that method here. Consequently, this paper is limited to a comparison of the hydrodynamic force acting on the particles arising from the single particle–pore interaction with the interparticle colloidal interaction. How this omission affects the calculations is discussed at the end of this section. In a future publication we will report calculations studying the simultaneous arrival of two and three particles at the entrance to a cylindrical pore, taking into account both interparticle and particle–pore hydrodynamic interactions (Ramachandran & Fogler 1999).

The hydrodynamic force acting on the particles was estimated using the results of Yan *et al.* (1987) who have studied the three-dimensional hydrodynamic interaction of a finite sphere with a circular orifice for low-Reynolds-number flows. Their

calculations are applicable here because the flow exterior to the pore is not significantly affected by the length of the pore (Dagan, Weinbaum & Pfeffer 1982). The hydrodynamic force components and the torque are given by:

$$F_x = 6\pi\mu a (U_x F_x^{t,x} + U_z F_x^{t,z} + a\Omega F_x^r + V_{z0} \tilde{F}_x^s), \quad (9)$$

$$F_z = 6\pi\mu a (U_x F_z^{t,x} + U_z F_z^{t,z} + a\Omega F_z^r + V_{z0} \bar{F}_z^s), \quad (10)$$

$$T_y = 8\pi\mu a^2 (U_x T_y^{t,x} + U_z T_y^{t,z} + a\Omega T_y^r + V_{z0} \bar{T}_y^s), \quad (11)$$

where V_{z0} is the fluid velocity at the centre of the orifice, and $F_x^{t,x}, F_x^{t,z}, \dots, \bar{T}_y^s$ are the 12 force and torque correction factors with superscripts t, r, s denoting the three problems mentioned above in sequence. In the expressions for the force and torque components, $F_x^{t,x}$ is the correction for the hydrodynamic force acting on the particle in the x -direction owing to translation in the x -direction. The term $F_x^{t,z}$ represents the cross-coupling effect, i.e. the hydrodynamic force acting on the particle in the x -direction owing to translation in the z -direction. When the particle is located at the pore axis or far away from the pore, $F_x^{t,z}$ vanishes. The notation for the other coefficients have similar interpretations.

In equations (10) and (11), the last terms on the right-hand side represent the component of the applied shear force acting on the particle. It is these components of the total hydrodynamic force that move the particle towards the pore and opposes the colloidal force acting on it. The other terms represent the drag experienced by the particle as it approaches the pore.

For an aspect ratio of 2, Yan *et al.* (1987) have calculated the force and torque coefficients as a function of position (discrete points) from the three-dimensional solution of the Stokes equations. They have also proposed approximate interpolation formulae for calculating the coefficients at any spatial location (and other aspect ratios). These formulae are listed in the Appendix. Numerical solutions of Yan *et al.* (1987) show that the correction factors $F_z^{t,z}, F_x^{t,x}, F_z^s$ and T_y^r are of the order of unity while the others are one order of magnitude smaller.

These hydrodynamic correction factors have been calculated more accurately by Wu *et al.* (1992). The results of Yan *et al.* (1991) have been used in this paper because of two reasons: (i) for the ranges of particle positions considered in the calculations, the critical Reynolds numbers for bridging estimated using the correction factors from the two papers are approximately the same, and (ii) the interpolation formulae provided by Yan *et al.* can be conveniently incorporated in the calculations. The first reason is discussed in more detail at the end of Appendix B.

4.3. Particles trajectories

The input to the trajectory calculations includes the initial positions of the particles, flow velocity, particle size, aspect ratio, zeta potential, and ionic strength. Particles of equal size and identical surface charge are considered here. The first step in the calculations involves the determination of the colloidal force acting on the particles using equations (5)–(7) given the particle positions. Next, the hydrodynamic force and torque correction factors are calculated using the expressions (B 2)–(B 8) (Appendix B). From a knowledge of the total colloidal force, the positions of the particles, and the hydrodynamic force and torque correction factors, the velocities of the particles are then calculated by simultaneously solving the force balance equations (2)–(4). These velocities are then substituted in equation (1) to determine the new positions of the particles. The new particle position is determined by specifying a displacement in the z -direction and calculating the displacement in the x -direction using equation

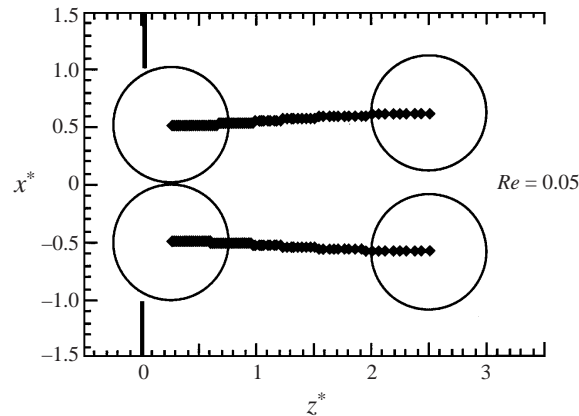


FIGURE 18. Trajectories of particles showing bridging at sufficiently high Re .

(1). This series of steps is repeated until the particles reach the final specified distance from the pore. The separation between the particles is determined for every $(x_i, 0, z_i)$.

Figure 18 shows the trajectories of two particles for a case where bridging is possible. Labels x^* and z^* denote distances along the x - and z -directions, respectively, scaled with the pore radius. The two thick lines at $z^* = 0$ represent the membrane surface surrounding the pore; the pore entrance therefore lies in the region $\{(x^*, y^*, 0) : (x^{*2} + y^{*2}) \leq 1\}$. A particle radius of $0.25 \mu\text{m}$, pore radius of $0.5 \mu\text{m}$ (aspect ratio = 2), particle zeta potential of -50 mV and an ionic strength of 0.001 M (monovalent electrolyte) were used. In the trajectory calculations, the two particles are initially equidistant from the pore wall and the pore axis. Under these conditions, a flow velocity corresponding to a Reynolds number of at least 0.05 is required to overcome the interparticle colloidal repulsion and cause bridging. Note that this value of Re falls well inside the Stokes regime. While interparticle contact is evident in figure 18, contact between the particles and the pore wall is absent since the van der Waals attraction between the particle and the membrane has not been included in the calculations. For values of $Re > 0.05$, the particles will be able to flocculate upstream of the pore entrance and will subsequently plug the pore. Figure 19 shows a situation where the particles are unable to bridge at the pore entrance because the Reynolds number is less than 0.05 (for example, $Re = 0.0025$). In the calculations shown in figures 18 and 19, only the magnitude of the fluid flow rate is different.

In figure 20, the interparticle separation distance (h) is shown as a function of the distance between the particle(s) and the plane of the pore for the two cases shown in figures 18 and 19. When the interstitial velocity corresponds to a Reynolds number of 0.05, the separation between the particles decreases to virtually zero at the pore entrance indicating that bridging will occur. When the Reynolds number is 0.0025, which is much less than the critical value of 0.05, the net electrostatic repulsion dominates over the applied shear force at the pore entrance. Consequently, the separation distance between the particles does not decrease to zero indicating their inability to bridge.

An intriguing observation from figure 19 is that the particles cannot pass through the pore even for the low Reynolds numbers considered; this observation suggests that plugging will occur for any non-zero flow velocity of the suspension through the membrane. However, experimental observations in regime I clearly show that plugging does not occur at velocities below the critical velocity. This contradiction

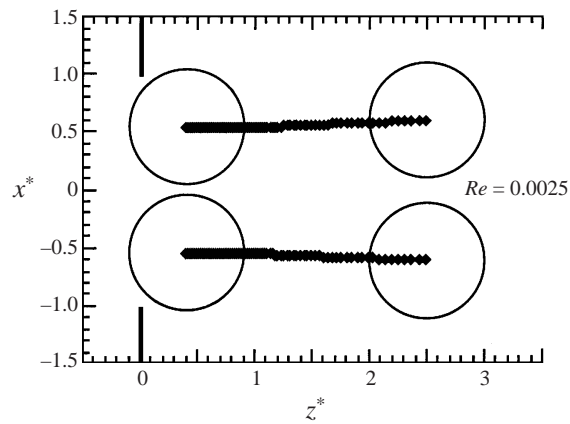


FIGURE 19. Trajectories of particles showing the inability to bridge if Re is insufficient.

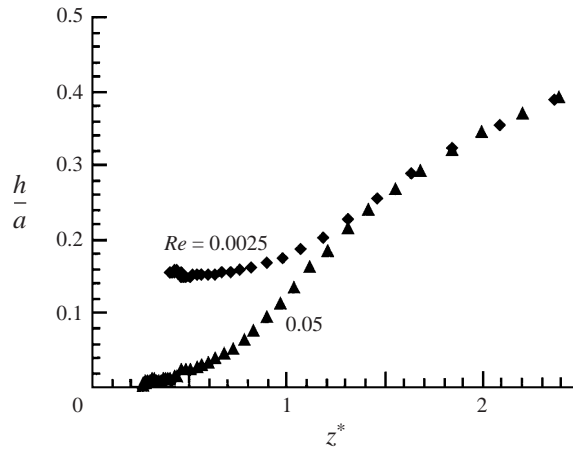


FIGURE 20. Surface separation between particles as they approach the pore for the two cases shown in figures 19 and 20.

can be resolved by realizing that the perfect symmetry in terms of the flow field through the pore and the particle positions assumed in the initial conditions is unlikely, even in model experimental systems such as that used here. The fact that asymmetry in the specified initial conditions will allow the particles to flow through the pore is illustrated in figure 21 where, initially, the particles are offset with respect to each other in the z -direction. The degree of offset required for the particles to flow through without plugging the pore is determined by the flow velocity. Specifically, it is expected that at high velocities large offsets in the initial particle positions are necessary for the particles to flow through the pore. This issue is discussed in detail in a future publication (Ramachandran & Fogler 1999).

The omission of the interparticle hydrodynamic forces in the calculations will affect the results of the trajectory calculations primarily in two ways: the applied hydrodynamic force causing particle motion towards the pore and towards one another will be different, and the lubrication forces arising owing to the slow drainage of the liquid between the particles will oppose their close approach. From a consideration of the physics of the situation, it is possible to predict how neglecting these two

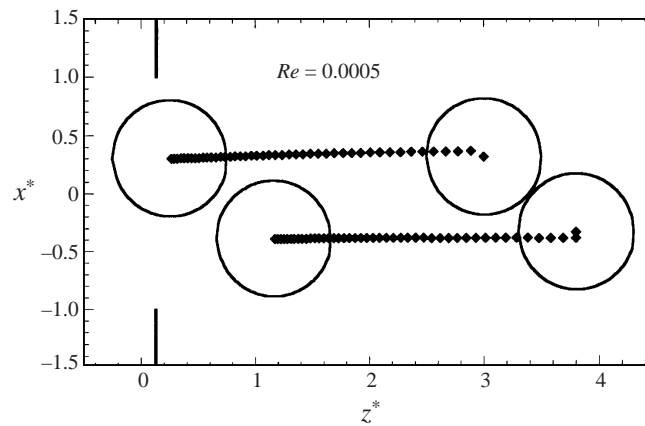


FIGURE 21. Ability of particles to flow through the pore without plugging when there is an offset in the initial particle positions.

interactions will affect the results. For the arrangement considered in the trajectory calculations, the presence of a second particle will probably increase the applied hydrodynamic force pushing the particle towards the pore. In the calculations, the use of mobility functions that include the interparticle hydrodynamic interactions near the pore will therefore result in a smaller critical Reynolds number required for bridging. The lubrication force arising when the particles are close to and moving towards each other will, however, have an opposite effect on the results because they tend to decrease the rate at which the particles are approaching each other. It is well known that this lubrication force becomes appreciable only for small interparticle separations. The reason why particle aggregation is possible in spite of the lubrication resistance is that the interparticle van der Waals attraction also becomes significant at these small separations. In terms of the results presented here, accounting for this lubrication force will tend to increase the critical Reynolds number required for bridging. The net effect of including the interparticle hydrodynamic interaction can only be determined by solving the hydrodynamic problem exactly. Other areas where a similar approximation has been made are the modelling of particle flocculation in unbounded fluid systems and particle deposition from flowing suspensions. Early studies in this area neglected both the interparticle van der Waals attraction and the lubrication resistance (van de Ven 1989; see §§ 5.1.6.1 and 6.3.3.2). The results from such studies were reasonable in spite of those seemingly egregious omissions because of the opposing influences of those interactions.

5. Conclusions

Particle retention by the mechanism of hydrodynamic bridging during the low-Reynolds-number flow of dilute, stable suspensions within cylindrical pores has been demonstrated experimentally. This mechanism can cause severe particulate plugging of porous media in the absence of retention by the conventional mechanisms of straining and deposition. It is the competition between hydrodynamic forces acting on particles near the pore entrance and the interparticle and particle-pore surface colloidal repulsion that determines the extent of particle retention by bridging. Experiments show that a critical velocity is required for particle retention to occur, and the magnitude of this critical velocity depends on the aspect ratio (ratio of pore size to

particle size), particle and pore surface properties, ionic strength, and pH. The effect of increasing the flow velocity on retention by bridging is to increase the rate of retention. This effect of velocity is opposite to that observed when only deposition occurs in the system studied.

Approximate calculations of the trajectories of two particles as they approach a cylindrical pore show that bridging in the Stokes regime is indeed possible for the experimental conditions in regime I. Quantitative information cannot be obtained from these calculations because particle–pore colloidal interaction and, more crucially, interparticle hydrodynamic interaction near the pore entrance have not been included. These interactions have not been included primarily because of the discontinuous nature of the pore entrance geometry. Though calculations shown here cannot provide accurate quantitative information, they do provide an order of magnitude estimate of the Reynolds number required for bridging in regime I. Furthermore, they serve the purpose of highlighting problems in colloidal hydrodynamics that must be solved for understanding the microfiltration of colloidal particles. A knowledge of such microscopic flow behaviour is imperative for understanding several important processes involving particulate flow through porous media.

Appendix A

In this Appendix, the extent of flocculation within pores is estimated for experimental conditions in regime I. In general, the extent of flocculation of a monodisperse suspension of particles in a shear flow field based on Smoluchowski's theory is given by

$$\frac{N}{N_0} = \exp(-4\alpha\phi Gt/\pi), \quad (\text{A } 1)$$

where N_0 is the initial number concentration of particles, N is the concentration of particles at time t , α is the collision efficiency (fraction of particle collisions that result in flocculation), ϕ is the volume fraction of particles, and G is the fluid shear rate. If the flocculation occurs during the laminar flow of the suspension within a cylindrical tube, Gt in equation (A 1) can be replaced by its flow-weighted average value in the tube (Gregory 1981a):

$$\bar{G}t = \frac{8L}{3R}, \quad (\text{A } 2)$$

where L and R are the length and the radius of the tube, respectively. The reduction in particle concentration due to tube flocculation then becomes:

$$\frac{N}{N_0} = \exp(-32L\alpha\phi/3\pi R). \quad (\text{A } 3)$$

As pointed out by Gregory (1981a), use of this mean value of Gt results in the overprediction of the extent of flocculation. However, for the purpose of checking whether shear induced flocculation within pores is significant in regime I, it will suffice to use the above expression. For experiments in regime I, $R = 0.41 \mu\text{m}$, $L = 10 \mu\text{m}$, and the maximum value of ϕ is of the order of 0.001. Equation (A 3) then becomes:

$$\frac{N}{N_0} = \exp(-0.083\alpha). \quad (\text{A } 4)$$

The collision efficiency α is a function of the flow geometry, shear rate, particle surface potential, ionic strength, and pH. For simple flow geometries, α can be

determined theoretically by computing the trajectories of particles incorporating both hydrodynamic and colloidal interactions. As would be intuitively expected, α increases with increasing interparticle attraction and shear rate. Analytical expressions for α are, however, not available for the case of Poiseuillean flow of colloidally stable particles. Van de Ven & Mason (1976) have numerically calculated α for flocculation in a simple shear field under conditions when both van der Waals attraction and electrostatic repulsion are significant. For a monodisperse suspension of particles, α is a function of dimensionless parameters C_A , C_R , and κa (see van de Ven & Mason 1976 for equations for C_A and C_R). C_A and C_R are measures of van der Waals attraction and double-layer repulsion, respectively, relative to the applied shear force and κa is the ratio of the particle radius to the double-layer thickness.

For experiments in regime I, the calculated values of C_A and C_R based on an interstitial velocity of 1 cm s^{-1} are 0.0011 and 2, respectively; the value of κa is about 1350. C_R being greater than 1 implies that the magnitude of the electrostatic repulsion is of the same order of magnitude of but greater than the applied shear force. The ratio C_R/C_A is about 1820 which indicates that double-layer repulsion is very strong relative to van der Waals attraction. Although α has not been calculated exactly for these values of the dimensionless parameters by van de Ven and Mason, it is still possible to ascertain whether flocculation will be significant in the experiments based on their work. Their calculations show that for $\kappa a = 300$, $C_A \approx 0.001$, and equal sized particles, the calculated value of α decreases from about 0.2 to less than 0.01 when C_R/C_A increases from 0 to 1.14. The value of α corresponding to experimental conditions in regime I will therefore be much less than 0.01 because C_R/C_A for the system is three orders of magnitude greater than the value used in the calculations of van de Ven and Mason. Note that for $\alpha = 0.01$, the extent of tube flocculation, $(1 - N/N_0)$, will be only about 0.8%. Because α is much less than 0.01 in the experiments, the extent of flocculation within pores will be negligible and therefore is not a factor in the experiments.

Appendix B

The expressions for the force and torque coefficients from Yan *et al.* (1987) used in the trajectory calculations are listed here. These interpolation formulae are valid for $z_0/a \geq 1.1$ where z_0 is the unscaled distance of the centre of a particle from the plane of the pore and a is the particle radius, and for a wide range of particle sizes. In the expressions, distances have been scaled with the pore radius and α is the aspect ratio.

$$F_x^{t,x} = (F_{x_{z_0}}^{t,x} - F_{x_0}^{t,x}) \left[1 - \operatorname{sech} \left(0.6 \frac{x}{(z\alpha)^{1/3}} \right) \right] + F_{x_0}^{t,x}, \quad (\text{B } 1)$$

$$F_x^{t,z} = \frac{(0.473z\alpha + 0.0172)x F_{x_1}^{t,z}}{x^4 + 0.43z\alpha}, \quad (\text{B } 2)$$

$$F_x^r = F_{x_{z_0}}^r + \frac{0.3(z\alpha)^{-2.5}x^3 + F_{x_0}^r - F_{x_{z_0}}^r}{x^4 + 1}, \quad (\text{B } 3)$$

$$\bar{F}_x^s = \frac{[3.6(z\alpha)^{0.9} + 0.225]x \bar{F}_{x_1}^s}{x^2 + 0.9(z\alpha)^{0.9}}, \quad (\text{B } 4)$$

$$F_z^r = \frac{[49.536(z\alpha)^{-4.5} + 0.0225]x^3 F_{z_1}^r}{x^5 + 2.15(z\alpha)^{-4.5}}, \quad (\text{B } 5)$$

$$T_y^r = (T_{y\infty}^r - T_{y0}^r) \left[1 - \operatorname{sech} \left(0.8 \frac{X}{(z\alpha)^{1/4}} \right) \right] + T_{y0}^r, \quad (\text{B } 6)$$

$$\bar{T}_y^s = \frac{[12(z\alpha)^{-1/2} + 0.0625]x\bar{T}_{y1}^s}{x^3 + 3(z\alpha)^{-1/2}}. \quad (\text{B } 7)$$

In the expressions, the subscript 0 denotes the axisymmetric values for a sphere near the orifice (i.e. $x = 0$) calculated by Yan *et al.*, the subscript ∞ denotes the far-field values for a sphere near an infinite solid plane wall which are obtained from Goldman, Cox & Brenner (1967), and the subscript 1 denotes values at $x = 0.25$ calculated by Yan *et al.* $F_z^{t,z}$ and F_z^s were obtained using bilinear interpolation from tables 3 and 4, respectively, in Wang *et al.* (1986). The rest of the force and torque coefficients are determined using the reciprocal theorem (Happel & Brenner 1973) as shown below:

$$F_z^{t,x} = F_x^{t,z}, \quad T_y^{t,x} = \frac{3}{4}F_x^r, \quad T_y^{t,z} = \frac{3}{4}F_z^r. \quad (\text{B } 8)$$

As mentioned previously, Wu *et al.* (1992) have calculated the above hydrodynamic correction factors more accurately. They have shown in their paper that their values for F_z^s and $F_z^{t,z}$, the correction factors that affect particle motion the most, match well with those of Yan *et al.* for $\alpha = \frac{1}{2}$. However, they found that Yan *et al.*'s calculated values for the cross-coupling resistance coefficients $F_x^{t,z}$ and $F_z^{r,y}$ are inaccurate. The errors were largest when the particles were near the plane of the pore (small z_0) and they decrease as z_0 increases. To determine the sensitivity of the calculated critical velocities to the magnitudes of these cross-coupling resistance coefficients, the trajectory calculations were repeated after multiplying Yan *et al.*'s numbers by the largest deviation in the range of particle positions considered. For example, the largest factor by which the value of $F_z^{t,z}$ calculated by Yan *et al.* deviates from that calculated by Wu *et al.* for $0.5 < x_0 \leq 0.6$ is 3.563 at $z_0 = 1.1$ (see table 4, p. 502 of Wu *et al.*). When the $F_z^{t,z}$ and $F_x^{t,z}$ magnitudes are increased by a factor of 4 in the calculations, the estimated critical Reynolds number was 0.04 as compared to a value of 0.05 obtained previously. Note that the maximum deviation of 4 to $F_z^{t,z}$ for all (x_0, z_0) applied in the calculation which is an over-correction. The sensitivity to $F_z^{r,y}$ was similarly checked and it was found that the use of the corrected value of the resistance coefficient did not change the calculated critical Reynolds number.

REFERENCES

- ADAMCZYK, Z., SIWEK, B. & SZYK, L. 1995 Flow-induced surface blocking effects in adsorption of colloid particles. *J. Colloid Interface Sci.* **174**, 130.
- ADAMCZYK, Z., SIWEK, B., ZEMBALA, M. & BELOUSCHEK, P. 1994 Kinetics of localized adsorption of colloidal particles. *Adv. Colloid Interface Sci.* **48**, 151.
- BHATTACHARJEE, S. & SHARMA, A. 1995 Lifshitz-van der Waals energy of spherical particles in cylindrical pores. *J. Colloid Interface Sci.* **171**, 288.
- BISIO, P. D., CARTLEDGE, J. G., KEESOM, W. H. & RADKE, C. J. 1980 Molecular orientation of aqueous surfactants on a hydrophobic solid. *J. Colloid Interface Sci.* **78**, 225.
- BOHRER, M. P. 1983 Diffusional boundary layer resistance for membrane transport. *Ind. Engng Chem. Fundam.* **22**, 72.
- BOWEN, W. R. & SHARIF, A. O. 1996 The hydrodynamic and electrostatic interaction on the approach and entry of a charged spherical particle to a charged cylindrical pore in a charged planar surface with implications for membrane separation processes. *Proc. R. Soc. Lond.* **452**, 2121.
- BOWEN, W. R. & SHARIF, A. O. 1997 Adaptive finite-element solution of the non-linear Poisson-Boltzmann equation: a charged spherical particle at various distances from a charged cylindrical pore in a charged planar surface. *J. Colloid Interface Sci.* **187**, 363.
- BRADY, J. F. & BOSSIS, G. 1988 Stokesian dynamics. *Ann. Rev. Fluid Mech.* **20**, 111.

- CHARLES, G. E. & MASON, S. G. 1960 The coalescence of liquid drops with flat liquid/liquid interfaces. *J. Colloid Interface Sci.* **15**, 236.
- DABROS, T. 1989 Interparticle hydrodynamic interactions in deposition processes. *Colloids Surfaces* **39**, 127.
- DAGAN, Z., WEINBAUM, S. & PFEFFER, R. 1982 An infinite-series as solution for the creeping motion through an orifice of finite length. *J. Fluid Mech.* **115**, 505.
- DAS, S. K., SCHECHTER, R. S. & SHARMA, M. M. 1994 The role of surface roughness and contact deformation on the hydrodynamic detachment of particles from surfaces. *J. Colloid Interface Sci.* **164**, 63.
- DAVIS, C. N. 1973 *Air Filtration*. Academic.
- DERJAGUIN, B. & LANDAU, L. 1941 Theory of the stability of strongly charged lyophobic sols and the adhesion of strongly charged particles in solutions of electrolytes. *Acta Physicochem.* **14**, 633.
- DURLOFSKY, L. & BRADY, J. F. 1989 Dynamic simulation of bounded suspensions of hydrodynamically interacting particles. *J. Fluid Mech.* **200**, 39.
- FEKE, D. L., PRABHU, N. D., AMIN JR, J. A. & AMIN II, J. A. 1984 A formulation of the short-range repulsion between spherical colloidal particles. *J. Phys. Chem.* **88**, 5735.
- FLEISCHER, R. L., PRICE, P. B. & WALKER, R. M. 1975 *Nuclear Tracks in Solids. Principles and Applications*. University of California Press, Berkeley.
- GLENDINNING, A. B. & RUSSEL, W. B. 1983 The electrostatic repulsion between charged spheres from exact solutions to the linearized Poisson–Boltzmann equation. *J. Colloid Interface Sci.* **93**, 95.
- GOLDMAN, A. J., COX, R. G. & BRENNER, H. 1967 Slow viscous motion of a sphere parallel to a plane wall – I Motion through a quiescent fluid. *Chem. Engng Sci.* **22**, 637–651.
- GREGORY, J. 1981a Flocculation in laminar tube flow. *Chem. Engng Sci.* **36**, 1789.
- GREGORY, J. 1981b Approximate expressions for retarded van der Waals interaction. *J. Colloid Interface Sci.* **83**, 131.
- GREGORY, J. 1982 Particle interactions in flowing suspensions. *Adv. Colloid Interface Sci.* **17**, 149.
- GRUESBECK, C. & COLLINS, R. E. 1982 Entrainment and deposition of fine particles in porous media. *J. Petrol. Technol.* **847**, December.
- HAPPEL, J. & BRENNER, H. 1973 *Low Reynolds Number Hydrodynamics*, p. 85. Noordhoff International Publishing, Leyden.
- HOFFMAN, J. A. M. H. & STEIN, H. N. 1992 Hydrodynamic and surface interaction forces on a particle in a pore. *J. Colloid Interface Sci.* **154**, 359.
- ISRAELACHVILI, J. N. 1985 *Intermolecular and Surface Forces – With Application to Colloidal and Biological Systems*. Academic.
- KAO, J., WANG, Y., PFEFFER, R. & WEINBAUM, S. 1988 A theoretical model for nuclepore filters including hydrodynamic and molecular wall interaction effects. *J. Colloid Interface Sci.* **121**, 543.
- KEESOM, W. H., ZELENKA, R. L. & RADKE, C. J. 1988 A zeta-potential model for surfactant adsorption on an ionogenic hydrophobic surface. *J. Colloid Interface Sci.* **125**, 575.
- KHILAR, K. C. & FOGLER, H. S. 1984 The existence of a critical salt concentration for particle release. *J. Colloid Interface Sci.* **101**, 214.
- LIABASTRE, A. A. & ORR, C. 1978 An evaluation of pore structure by mercury penetration. *J. Colloid Interface Sci.* **64**, 1.
- MCCARTHY, J. F. & WOBBER, F. J. (Eds.) 1994 *Manipulation of Groundwater Colloids for Environmental Restoration*. Lewis.
- MARTÍNEZ-VILLA, F., ARRIBAS, J. I. & TEJERINA, F. 1988 Quantitative microscopic study of surface characteristics of track-etched membranes. *J. Membrane Sci.* **36**, 19.
- MEINDERS, J. M., NOORDMANS, J. & BUSSCHER, H. J. 1992 Simultaneous monitoring of the adsorption and desorption of colloidal particles during deposition in parallel plate flow chamber. *J. Colloid Interface Sci.* **152**, 265.
- MELIK, D. H. & FOGLER, H. S. 1988 Fundamentals of colloidal stability in quiescent media. *Encyclopedia of Emulsion Technology*, vol. 3. Marcel Dekker.
- MUECKE, T. W. 1979 Formation fines and factors controlling their movement in porous media. *J. Petrol. Technol.* **144**, February.

- PAPADOPOULOS, K. D. & KUO, C. 1990 The van der Waals interaction between a colloid and its host pore. *Colloids Surfaces* **46**, 115.
- PAYATAKES, A. C. & GRADON, L. 1980 Dendritic deposition of aerosol particles in fibrous media by inertial impaction and interception. *Chem. Engng Sci.* **35**, 1083.
- PORTER, K. E. 1989 An overview of formation damage. *J. Petrol. Technol.* **780**, August.
- RAMACHANDRAN, V. & FOGLER, H. S. 1999 Low Reynolds number interactions between colloidal particles near the entrance to a cylindrical pore. In preparation.
- RUSSEL, W. B., SAVILLE, D. A. & SCHOWALTER, W. R. 1989 *Colloidal Dispersions*. Cambridge University Press.
- SCHENKEL, J. H. & KITCHENER, J. A. 1960 A test of the Derjaguin–Verwey–Overbeek theory with a colloidal suspension. *Trans Faraday Soc.* **56**, 161.
- SCOTT, K. 1990 *Membrane Separation Technology*. Scientific and Technical Information, Oxford.
- SMITH III, F. G. & DEEN, W. M. 1983 Electrostatic effects on the partitioning of spherical colloids between dilute bulk solution and cylindrical pores. *J. Colloid Interface Sci.* **91**, 571.
- SPIELMAN, L. A. 1977 Particle capture from low-speed laminar flows. *Ann. Rev. Fluid Mech.* **9**, 297.
- TADROS, TH. F. & GREGORY, J. (Eds.) 1994 *Colloids in the Aquatic Environment*. Elsevier.
- TIEN, C. 1989 *Granular Filtration of Aerosols and Hydrosols*. Butterworth.
- VAN DE VEN, T. G. M. 1989 *Colloidal Hydrodynamics*. Academic, San Diego.
- VAN DE VEN, T. G. M. & MASON, S. G. 1976 The microrheology of colloidal dispersions IV. Pairs of interacting spheres in shear flow. *J. Colloid Interface Sci.* **57**, 505.
- VERWEY, E. J. & OVERBEEK, J. TH. G. 1948 *Theory of the Stability of Lyophobic Colloids*. Elsevier.
- VITTHAL, S. & SHARMA, M. M. 1992 A Stokesian dynamics model for particle deposition and bridging in granular media. *J. Colloid Interface Sci.* **153**, 314.
- WANG, Y., KAO, J., WEINBAUM, S. & PFEFFER, R. 1986 On the inertial impaction of small particles at the entrance of a pore including hydrodynamic and molecular wall interaction effects. *Chem. Engng Sci.* **41**, 45.
- WU, W., WEINBAUM, S. & ACRIVOS, A. 1992 Shear flow over a wall with suction and its application to particle screening. *J. Fluid Mech.* **243**, 489.
- YAN, Z., ACRIVOS, A. & WEINBAUM, S. 1991 Fluid skimming and particle entrainment into a small circular side pore. *J. Fluid Mech.* **229**, 1.
- YAN, Z., WEINBAUM, S., GANATOS, P. & PFEFFER, R. 1987 The three-dimensional hydrodynamic interaction of a finite sphere with a circular orifice at low Reynolds number. *J. Fluid Mech.* **174**, 39.
- ZEICHNER, G. R. & SCHOWALTER, W. R. 1977 Use of trajectory analysis to study stability of colloidal dispersions in flow fields. *AIChE J.* **23**, 243.